Electronic Supplementary Material (ESI) for Analytical Methods.

Fabrication of 2D Metal-organic frameworks (MOFs) nanosheets and investigation its fluorescence response to pesticide molecules

Boya Su,[a] Shengyun Liao, [a,b,*] Haitao Zhu,[a] Shuxian Ge, [a] Yan Liu, [a] Jingyao Wang,[d] Hui Chen, [a,*] Lidong Wang [c,*]

[a] Tianjin Key Laboratory of Organic Solar Cells and Photochemical Conversion, Tianjin Key Laboratory of Drug Targeting and Bioimaging, School of Chemistry and Chemical Engineering, Tianjin University of Technology, No. 391 Binshuixi Road, Tianjin, 300384, China

[b] Key Laboratory of Advanced Energy Materials Chemistry (Ministry of Education), College of Chemistry, Nankai University, Tianjin, 300071, China

[c] Rotam CropScience Limited Company, No. 16 Huangshan Road, Modern Industrial Park, Hangu of TEDA, Tianjin, 300457, China

[d] Safety and Technical of Industrial Products Center, Tianjin Customs District, Tianjin, 300308, China

[*] Corresponding authors. E-mail: 18202587221@163.com (S. Liao), tjge@tjut.edu.cn (H. Chen), casiwang@rotam.com (L. Wang)

Table of contents

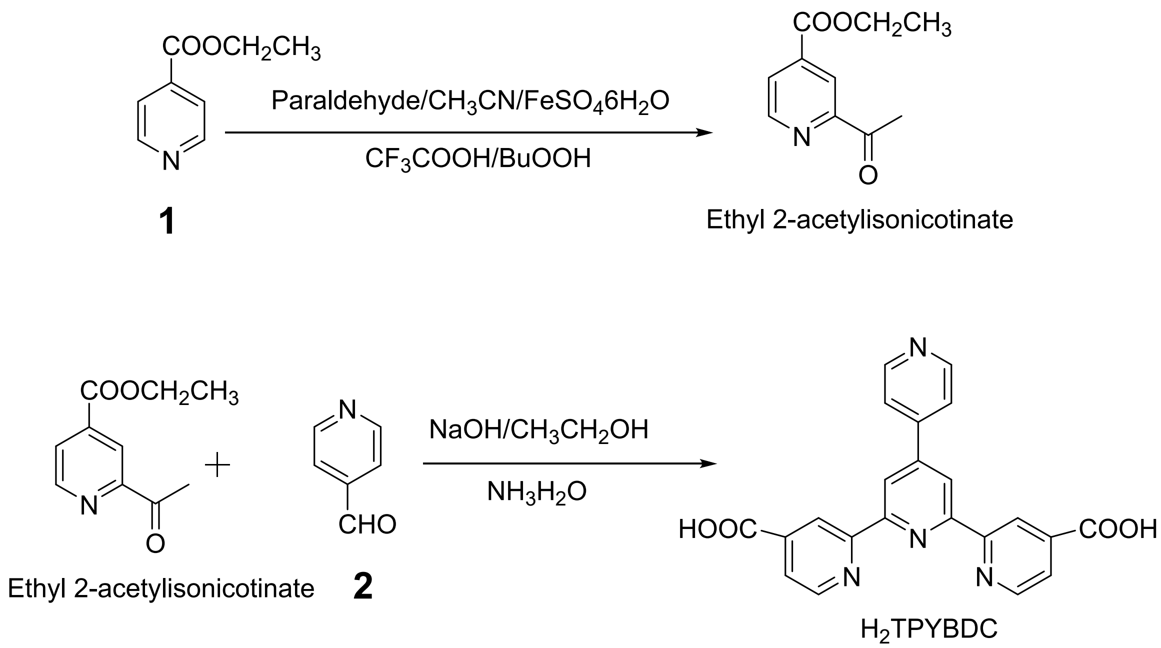

Scheme S1. The routine for Synthesis of $H_2TPYBDC$.

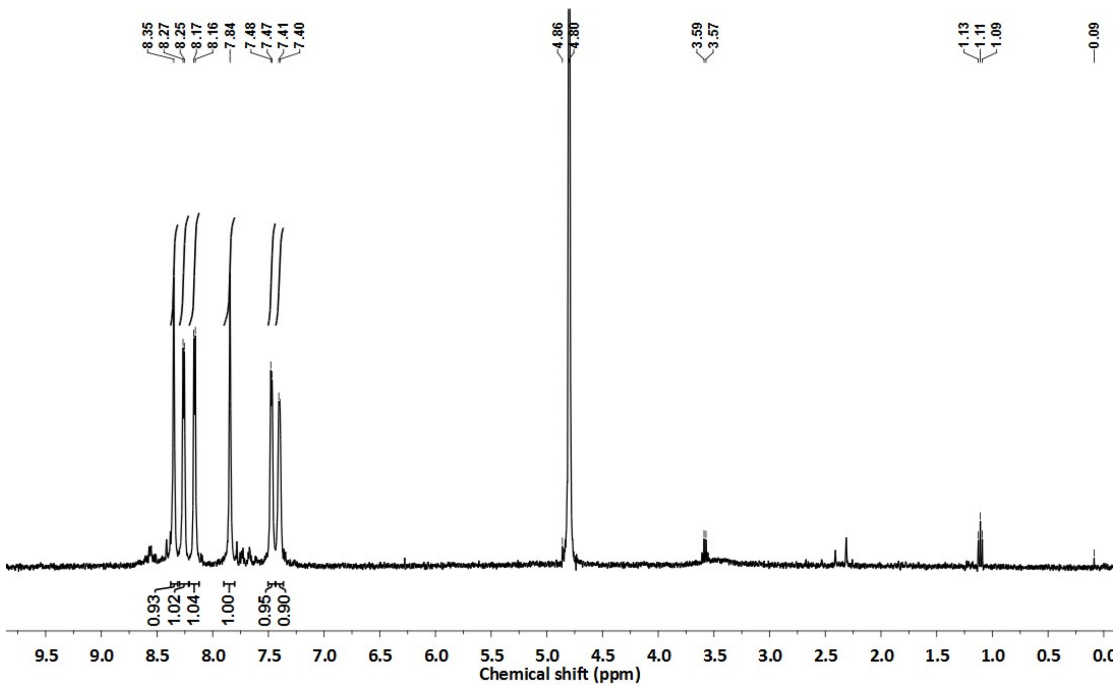

Figure S1. ${}^{1}HNMR$ spectra of $H_2TPYBDC$ (400 Hz, D_2O, 25 °C).

Table S1. Crystal data and structure refinement for Zn-LMOF.

Identification code	Zn-LMOF
Empirical formula	$C_{88}H_{56}N_{16}O_{20}Zn_4$
Formula weight	1918.96
Temperature/K	293(2)
Crystal system	monoclinic
Space group	P21/c
a/Å	7.9231(4)
b/Å	13.8107(6)
c/Å	17.1406(8)
α/°	90
β/°	102.171(5)
γ/°	90
Volume/Å^3	1833.43(15)
Z	1
ρ_{calc} g/cm^3	1.738
μ/mm^{-1}	1.388
F(000)	976.0
Crystal size/mm^3	0.20×0.20×0.20
Radiation	MoKα (λ = 0.71073)
2θrange for data collection/°	6.03 to 66.184
Index ranges	-11⩽h⩽8, -21⩽k⩽18, -24⩽l⩽24
Reflections collected	10152
Independent reflections	6153 [R_{int} = 0.0415, R_{sigma} = 0.0746]
Data/restraints/parameters	6132/0/292
Goodness-of-fit on F^2	0.990
Final R indexes [I> =2σ (I)]	R_1 = 0.0403, wR_2 = 0.1035
Final R indexes [all data]	R_1 = 0.0728, wR_2 = 0.1328
Largest diff. peak/hole / eÅ^{-3}	0.64/-0.85

Table S2. The main bond lengths and bond angles for Zn-LMOF.

Bond Lengths	Length/Å	Bond Angles	Angle/°
Zn1-O2	1.9711(16)	O2-Zn1-O3^{1}	103.59(8)
Zn1-O3^{1}	1.9840(17)	O2-Zn1-N2^{2}	147.97(7)
Zn1-N2^{2}	2.0821(18)	O2-Zn1-N1^{2}	88.29(7)
Zn1-N1^{2}	2.2020(18)	O2-Zn1-N3^{2}	109.55(7)
Zn1-N3^{2}	2.1589(18)	O3^{1} -Zn1-N2^{2}	104.15(8)
O3-Zn1^{3}	1.9839(17)	O3^{1} -Zn1-N1^{2}	94.38(7)
N2-Zn1^{4}	2.0821(18)	O3^{1} -Zn1-N3^{2}	109.45(7)
N1-Zn1^{4}	2.2019(18)	N2^{2} -Zn1-N1^{2}	73.96(7)
N3-Zn1^{4}	2.1590(18)	N2^{2} -Zn1-N3^{2}	75.54(7)
		N3^{2} -Zn1-N1^{2}	145.00(7)

^{1}1+x, 1/2-y, -1/2+z; ^{2}1-x, 1/2+y, 1/2-z; ^{3}-1+x, 1/2-y, 1/2+z; ^{4}1-x, -1/2+y, 1/2-z

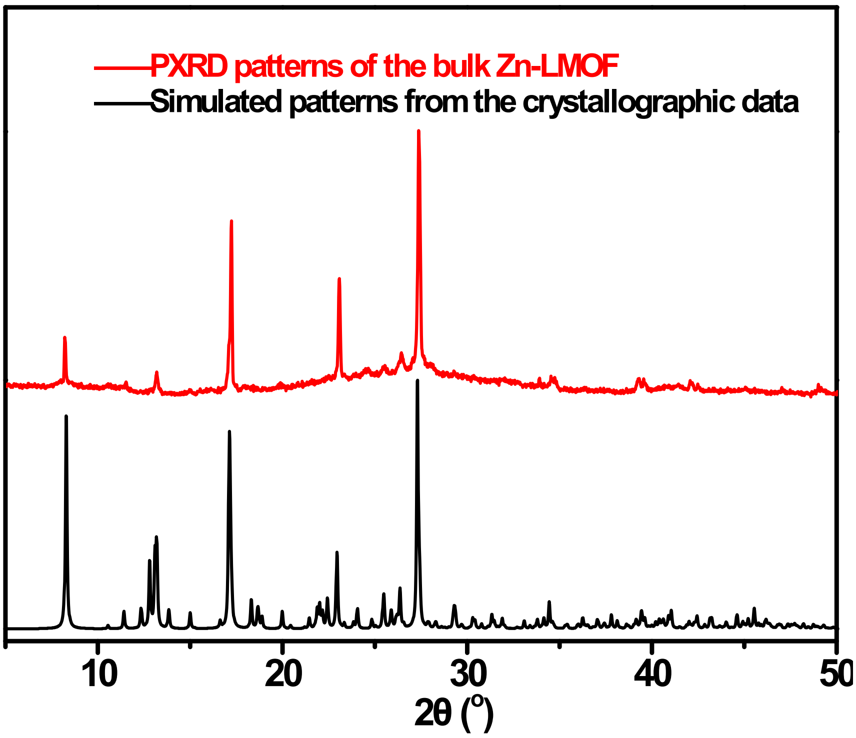

Figure S2. The PXRD patterns of the as-synthesized Zn-LMOF ([Zn(TPYBDC)·H_2O]$_n$).

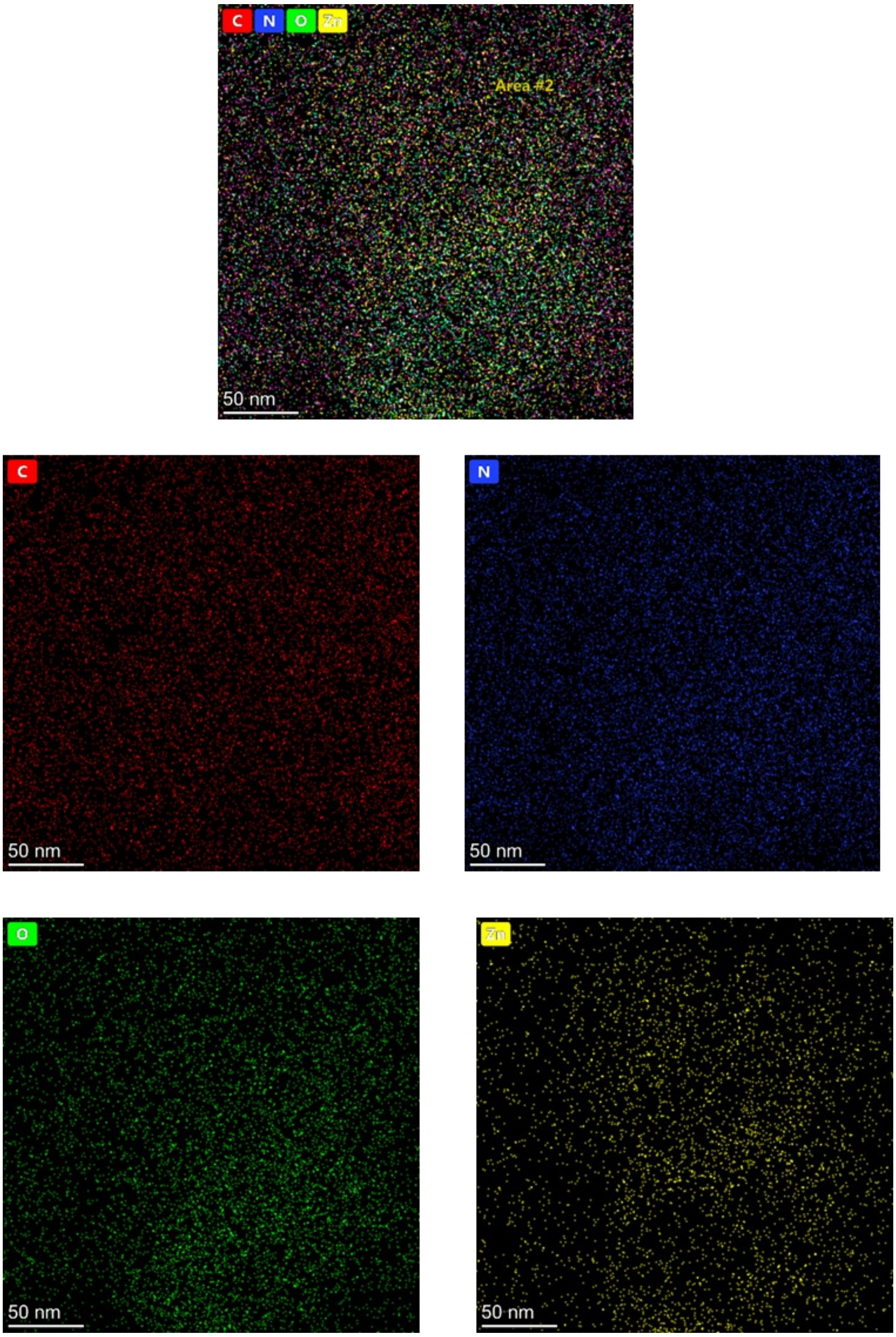

Figure S3. Elemental mapping of the 2D Zn-LMOF nanosheets colloidal.

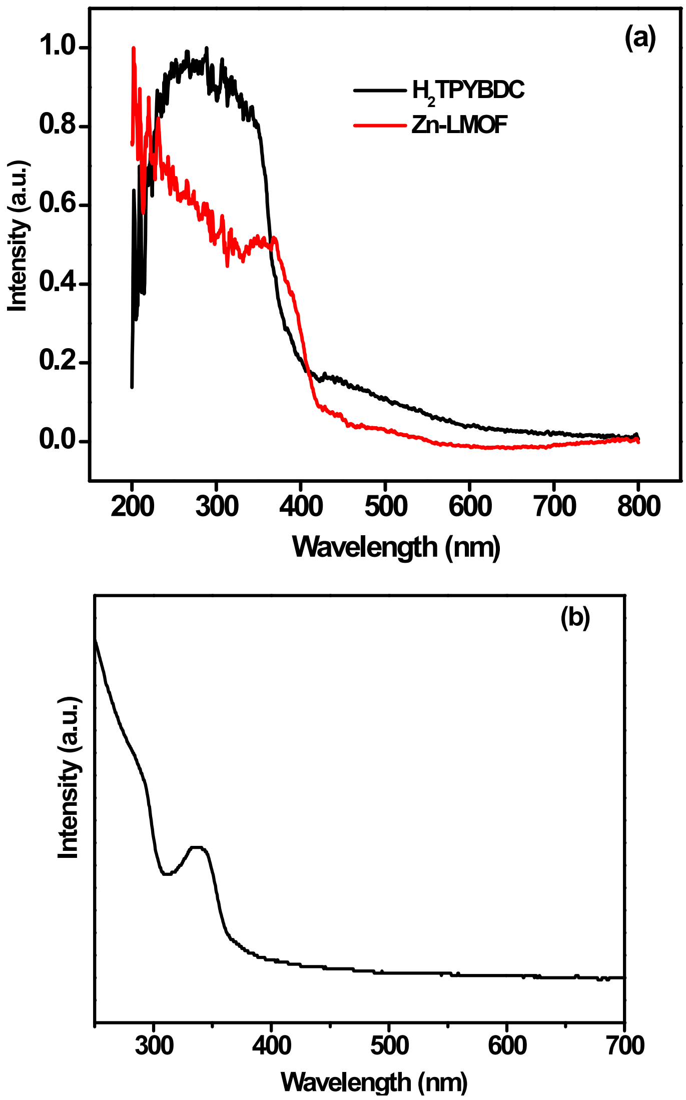

Figure S4. (a)The solid-state UV spectra of H_2TPYBDC and Zn-LMOF; (b) The UV spectrum of Zn-LMOF nanosheets colloidal.

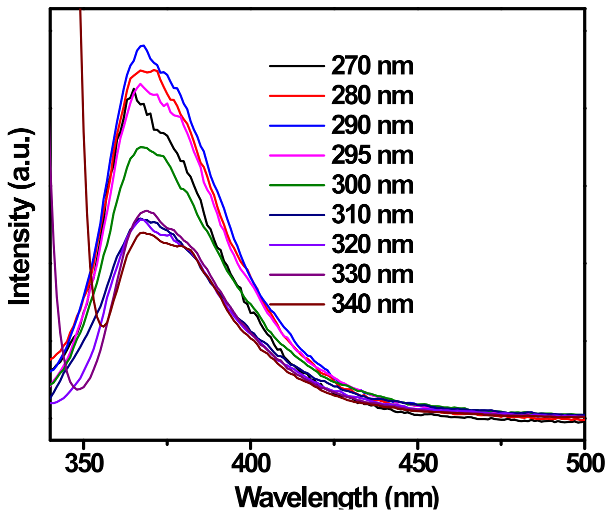

Figure S5. The emission spectra of the 2D Zn-LMOF nanosheets colloidal at different excitation wavelengths.

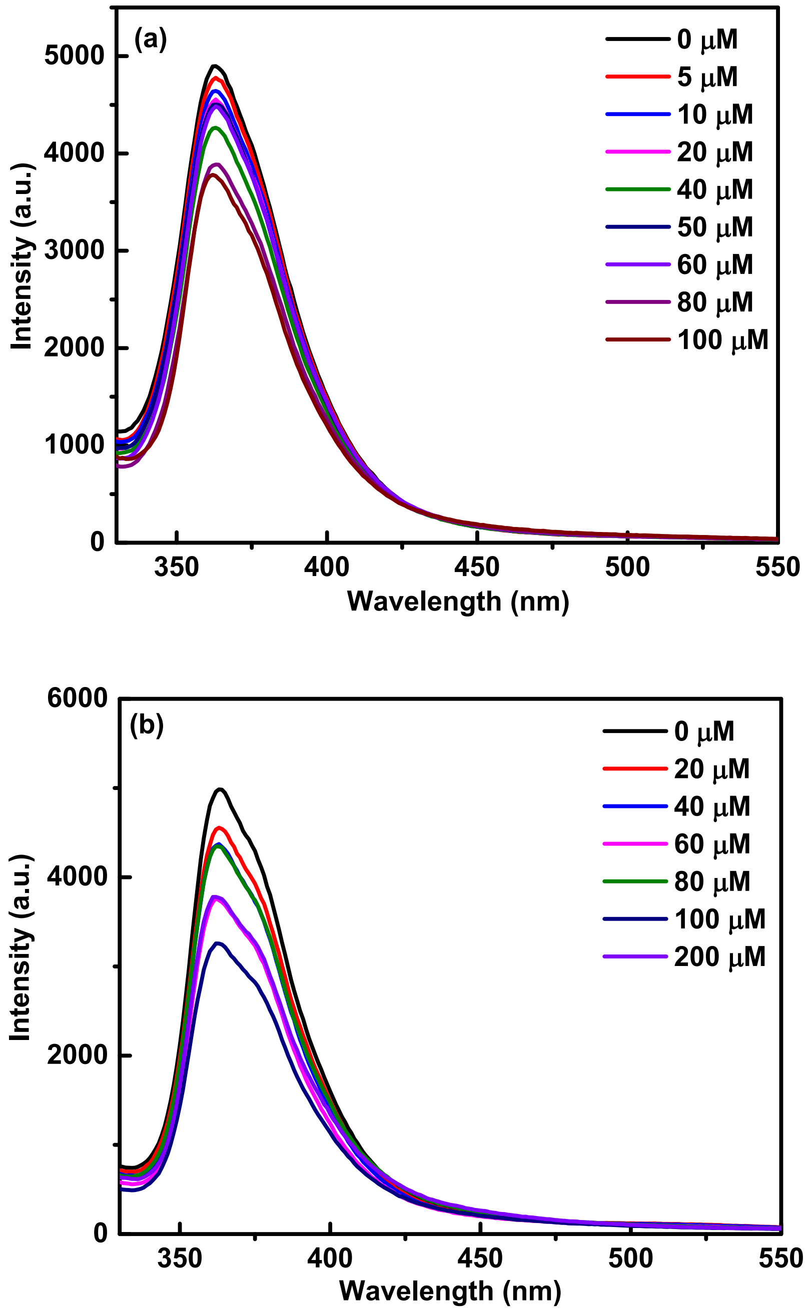

Figure S6. Fluorescence quenching response of Zn-LMOF nanosheets colloidal after adding (a) Glufosinate ammonium and (b) Glyphosate with various concentrations.

Table S3. Summary of the reported detection methods for imidacloprid, nitenpyram, and Dinotefuran.

Pesticides	Material	Methods	Medium	LOD	Ref.
Imidacloprid		HPLC	Water	0.005 mg/L	[S1]
	GO-UCNPs	Fluorescence resonance energy transfer (FRET) immunoassay	Phosphate buffered solution	0.08 ng/mL	[S2]
	Tyr-MoO_3 QDs	Fluorescence method	Phosphate buffered solution	4.00×10^{-9} M	[S3]
	$nAgn_f/nTiO_2n_f$ modified GCE	Electrochemical sensor	Britton-Robinson buffered solution	0.63×10^{-6} M	[S4]
	2D Zn-LMOF nanosheets colloidal	**Fluorescence method**	**Water**	**0.562 μM**	**This work**
Nitenpyram	In(III)/Tb(III)–MOF	Fluorescence method	Water	0.17 μg/mL	[S5]
		Surface Plasmon Resonance	Methanol	0.0085-0.11 μg/mL	[S6]
	β-cyclodextrin-reduced graphene oxide nanosheets	Electrochemical sensor	Phosphate buffered solution	0.3 μg/mL	[S7]
	2D Zn-LMOF nanosheets colloidal	**Fluorescence method**	**Water**	**0.441 μM**	**This work**
Dinotefuran	S-CQDs/CuNCs	Fluorescence method	Water	7.04 μM	[S8]
	b-CD-rGO/GCE	Electrochemical sensor	Phosphate buffered solution	0.01 mg/kg	[S9]
	Enzyme-linked immunosorbent assay (ELISA)	HPLC	Methanol	0.6 ng/mL	[S10]
		Rapid resolution liquid chromatography triples quadrupole tandem mass spectrometry (RRLC-MS/MS)	Acetonitrile	0.2 mg/kg	[S11]
	2D Zn-LMOF nanosheets colloidal	**Fluorescence method**	**Water**	**0.247 μM**	**This work**

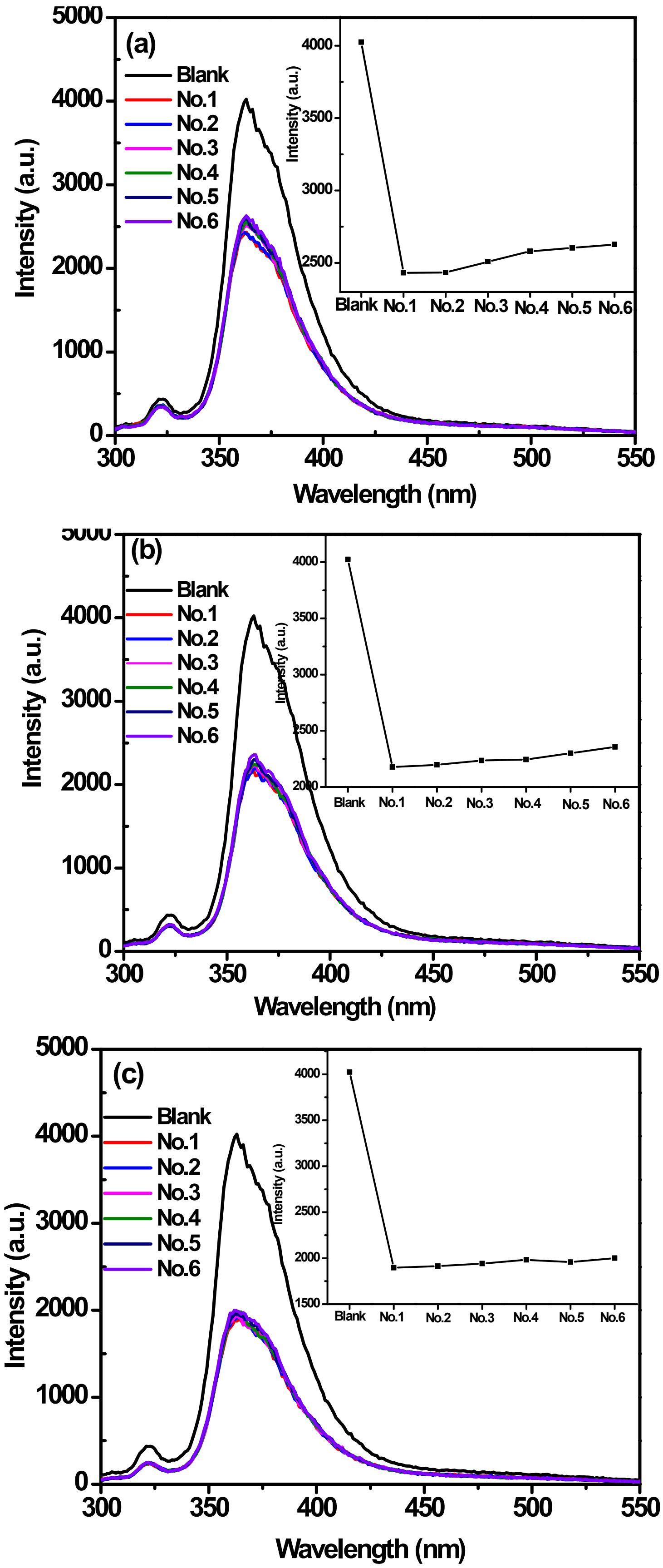

Figure S7. Fluorescence spectra of probes in river water with different concentrations of imidacloprid: (a) 50 μM; (b) 70 μM; (c) 100 μM (The insets are the correlation curves between the relative fluorescent intensity and the times).

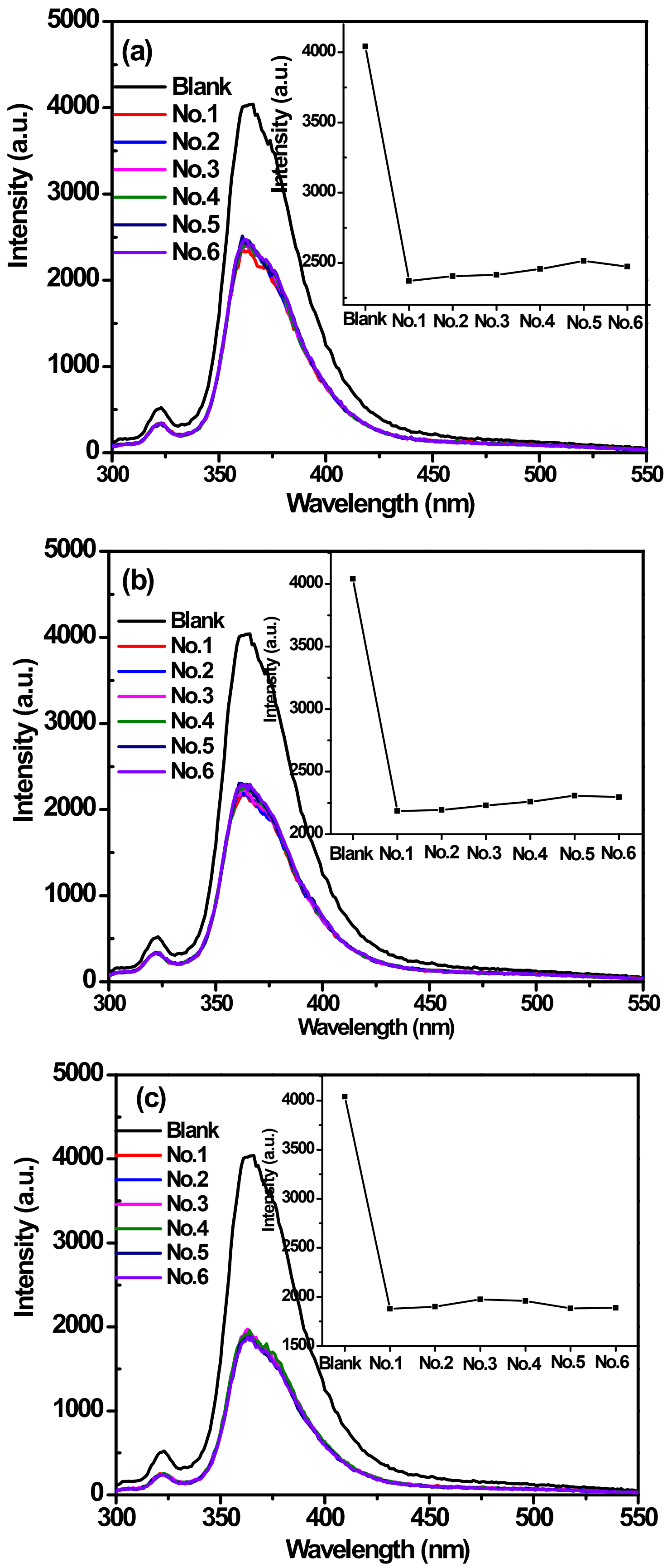

Figure S8. Fluorescence spectra of probes in tap water with different concentrations of imidacloprid: (a) 50 μM; (b) 70 μM; (c) 100 μM (The insets are the correlation curves between the relative fluorescent intensity and the times).

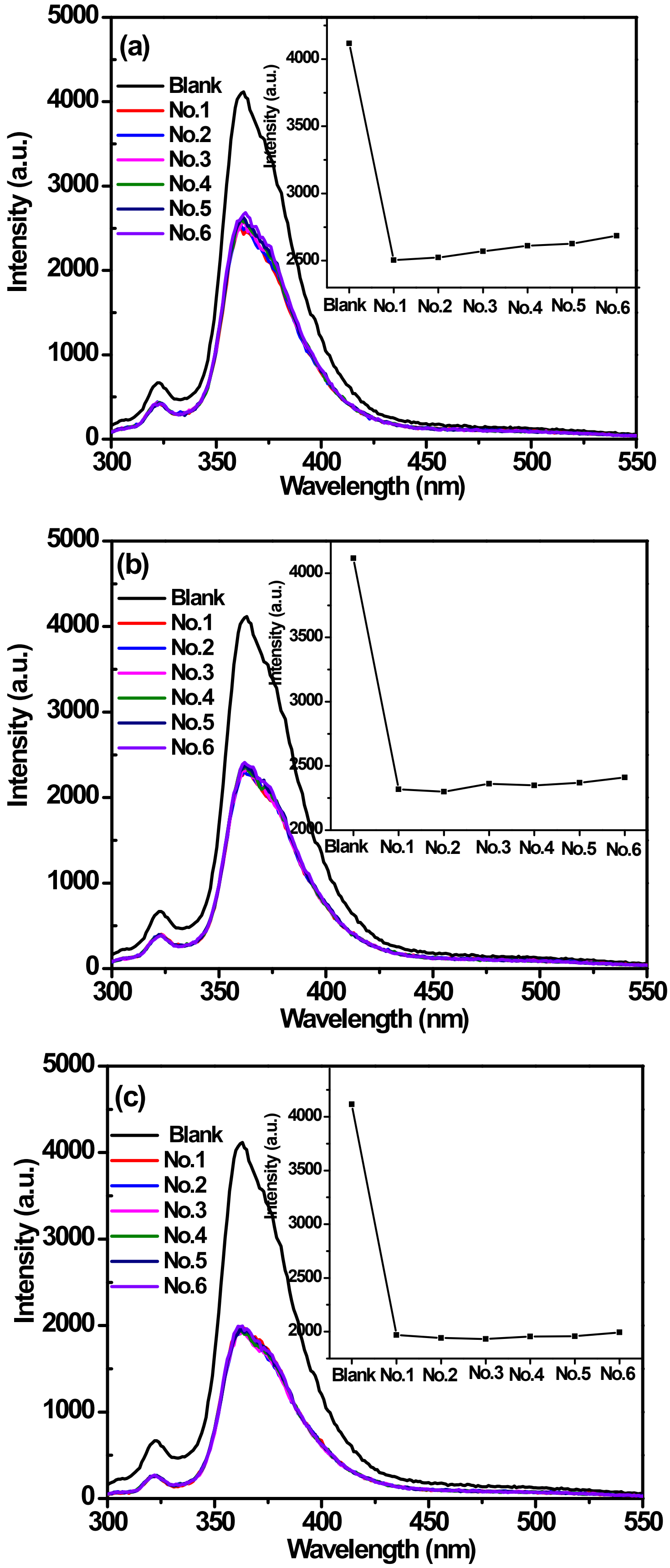

Figure S9. Fluorescence spectra of probes in Nongfu Spring with different concentrations of imidacloprid: (a) 50 μM; (b) 70 μM; (c) 100 μM (The insets are the correlation curves between the relative fluorescent intensity and the times).

Table S4. Analytical results (mean ±σ, n=6) for the detection of imidacloprid in domestic water.

Sample	Spiked/μM	Entry	I	Measured/μM	Average/μM	Recovery/%
River Water	100	1	1897	103.05	97.54	97.54
		2	1914	101.19		
		3	1942	98.19		
		4	1982	94.05		
		5	1957	96.61		
		6	2001	92.14		
	70	1	2177	76.04	70.09	100.13
		2	2198	74.29		
		3	2235	71.29		
		4	2244	70.58		
		5	2300	66.25		
		6	2357	62.06		
	50	1	2433	56.78	50.56	101.12
		2	2434	56.72		
		3	2509	51.82		
		4	2581	47.39		
		5	2604	46.03		
		6	2628	44.63		
Tap Water	100	1	1877	106.19	102.23	102.23
		2	1899	103.72		
		3	1975	95.61		
		4	1959	97.27		
		5	1883	105.51		
		6	1887	105.06		
	70	1	2185	76.14	71.34	101.91
		2	2193	75.47		
		3	2229	72.53		
		4	2259	70.14		
		5	2307	66.46		
		6	2296	67.29		
	50	1	2371	61.78	57.17	114.34
		2	2405	59.39		
		3	2414	58.77		
		4	2455	56.00		
		5	2513	52.24		
		6	2473	54.82		
Nongfu Spring	100	1	1969	100.05	101.22	101.22
		2	1941	103.04		
		3	1932	104.02		

		4	1956	101.43		
		5	1957	101.32		
		6	1994	97.45		
	70	1	2319	68.80	66.43	94.90
		2	2300	70.26		
		3	2361	65.68		
		4	2349	66.56		
		5	2369	65.10		
		6	2410	62.17		
	50	1	2504	55.82	50.71	101.42
		2	2523	54.59		
		3	2570	51.64		
		4	2610	49.21		
		5	2627	48.20		
		6	2686	44.79		

References

[S1] L. Li and Y. Cao , Determination of imidacloprid residues in farm water by HPLC, *Enterprise Technology Development*, 2010, **09** , 72-73.

[S2] Y. R. Guo , R. B. Zou , F. F. Si , W. L. Liang , T. Y. Zhang , Y. Y. Chang , X. S. Qiao and J. H. Zhao , A sensitive immunoassay based on fluorescence resonance energy transfer from up-converting nanoparticles and graphene oxide for one-step detection of imidacloprid, *Food Chemistry*, 2020, **335** , 127609.

[S3] M. R. Kateshiya , N. I. Malek and S. K. Kailasa , Facile synthesis of highly blue fluorescent tyrosine coated molybdenum oxide quantum dots for the detection of imidacloprid pesticide, *Journal of Molecular Liquids*, 2020, **319** , 114329.

[S4] A. Kumaravel and M. Chandrasekaran , Electrochemical determination of imidacloprid using nanosilver Nafion/nanoTiO_2 Nafion composite modified glassy carbon electrode[J], *Sensors and Actuators B: Chemical*, 2011, **158** , 319-326.

[S5] A. J. Li , Q. Q. Chu , H. F. Zhou , Z. P. Yang , B. Liu and J. W. Zhang , Effective nitenpyram detection in a dual-walled nitrogen-rich In(III)/Tb(III)-organic framework, *Inorganic Chemistry Frontiers*, 2021, **8** , 2341-2348.

[S6] S. Miyake , Y. Hirakawa , T. Yamasaki , E. Watanabe , A. Harada , S. Iwasa and H. Narita , Simultaneous detection of six different types of pesticides by an immunosensor based on surface plasmon resonance, *Analytical Sciences*, 2010, **36** , 335-340.

[S7] M. Zhang , H. Zhang , X. C. Zhai , X. Yang , H. T. Zhao , J. Wang , A. J. Dong and Z. Y. Wang , Application of β-cyclodextrin-reduced graphene oxide nanosheets for enhanced electrochemically sensing nitenpyram residue in real samples, *New Journal of Chemistry*, 2017, **41** , 2169-2177.

[S8] Y. Yang , Q. Y. Wei , T. Zou , Y. L. Kong , L. F. Su , D. Ma and Y. D. Wang , Dual-emission ratiometric fluorescent detection of dinotefuran based on sulfur-doped carbon quantum dots and copper nanocluster hybrid, *Sensors and Actuators B: Chemical*, 2020, **321** , 128534.

[S9] M. Zhang , X. C. Zhai , X. Yang , H. T. Zhao , A. J. Dong , H. Zhang , J. Wang and G.Y. Liu, Rapid and sensitive determination of dinotefuran residue based on electrochemical enhancement of β-cyclodextrin-graphene composite, *Electroanalysis*, 2016, **28** , 1-10.

[S10] E. Watanabe , K. Baba and S. Miyake , Analytical evaluation of enzyme-linked immunosorbent assay for neonicotinoid dinotefuran for potential application to quick and simple screening method in rice samples, *Talanta*, 2011, **84** , 1107-1111.

[S11] X. X. Chen , X. Z. Liu , B. Z. Dong and J. Y. Hu , Simultaneous determination of pyridaben, dinotefuran, DN and UF in eggplant ecosystem under open-field conditions: Dissipation behaviour and residue distribution, *Chemosphere*, 2018, **195** , 245-251.